Title
Diffusion and migration in polymer electrolytes

Authors
Choo, Youngwoo
Halat, David M
Villaluenga, Irune
et al.

Publication Date
2020-04-01

DOI
10.1016/j.progpolymsci.2020.101220

Peer reviewed

Diffusion and Migration in Polymer Electrolytes

*Youngwoo Choo [a], David M. Halat [a], Irune Villaluenga [a], Ksenia Timachova [a, b], Nitash P. Balsara [a, b, *]*

a. Materials Sciences Division and Joint Center for Energy Storage Research, Lawrence Berkeley National Laboratory, Berkeley, CA 94720, USA.

b. Department of Chemical and Biomolecular Engineering, University of California, Berkeley, CA 94720, USA

Abstract

Mixtures of neutral polymers and lithium salts have the potential to serve as electrolytes in next-generation rechargeable Li-ion batteries. The purpose of this review is to expose the delicate interplay between polymer-salt interactions at the segmental level and macroscopic ion transport at the battery level. Since complete characterization of this interplay has only been completed in one system: mixtures of poly(ethylene oxide) and lithium bis(trifluoromethanesulfonyl)imide (PEO/LiTFSI), we focus on data obtained from this system. We begin with a discussion of the activity coefficient, followed by a discussion of six different diffusion coefficients: the Rouse motion of polymer segments is quantified by D_{seg}, the self-diffusion of cations and anions is quantified by $D_{self,+}$ and $D_{self,-}$, and the build-up of concentration gradients in electrolytes under an applied potential is quantified by Stefan-Maxwell diffusion coefficients, $\mathfrak{D}_{0+}$, $\mathfrak{D}_{0-}$, and $\mathfrak{D}_{+-}$. The Stefan-Maxwell diffusion coefficients can be used to predict the velocities of the ions at very early times after an electric field is applied across the electrolyte. The surprising result is that $\mathfrak{D}_{0-}$ is negative in certain concentration windows. A consequence of this finding is that at these concentrations, both cations and anions are predicted to migrate toward the positive electrode at early times. We describe the controversies that surround this result. Knowledge of the Stefan-Maxwell diffusion coefficients enable prediction of the limiting current. We argue that the limiting current is the most important characteristic of an electrolyte. Excellent agreement between theoretical and experimental limiting current is seen in PEO/LiTFSI mixtures. What sequence of monomers that, when polymerized, will lead to the highest limiting current remains an important unanswered question. It is our hope that the approach presented in this review will guide the development of such polymers.

Keywords: Diffusion Coefficient, Migration, Polymer Electrolytes, Batteries, Ion Transport

Corresponding author: nbalsara@berkeley.edu

Table of Contents

Abbreviations

a	diameter of reptation tube
b	statistical segment length
c	salt concentration (mol/L)
c_{av}	average salt concentration (mol/L)
c_0	molar concentration of ethylene oxide monomers (mol/L)
c_T	total electrolyte concentration (mol/L)
D	salt diffusion coefficient (cm²/s)
D_{seg}	polymer segmental diffusion coefficient (cm^2/s)
$D_{self,+}$, $D_{self,-}$	self-diffusion coefficients of cation and anion measured by PFG-NMR (cm^2/s)
$\mathfrak{D}_{0+}$	Stefan-Maxwell diffusion coefficient describing the interactions between Li^+ and PEO (cm^2/s)
$\mathfrak{D}_{0-}$	Stefan-Maxwell diffusion coefficient describing the interactions between $TFSI^-$ and PEO (cm^2/s)
$\mathfrak{D}_{+-}$	Stefan-Maxwell diffusion coefficient describing the interactions between Li^+ and $TFSI^-$ (cm^2/s)
e_c	charge of an electron (1.602×10^{-19} C)
eNMR	electrophoretic NMR
F	Faraday constant (96485 C/mol)
$g_{Li\text{-}O}(r)$	Li-O radial distribution function
$g_{N\text{-}C}(r)$	N-C radial distribution function
i	constant-valued applied current density (mA/cm²)
iL	limiting current density (mA/cm)
k	Boltzmann constant (1.381×10^{-23} J/K)
l	Bjerrum length
L	electrolyte thickness (μm)
LiTFSI	lithium bis(trifluoromethanesulfonyl) imide
m	molality (mol/kg)
N	number of monomers per chain
PEO	poly(ethylene oxide)
PFG-NMR	pulsed-field gradient NMR
p_R	Rouse parameter
r	molar concentration of lithium ions to ether oxygens ($r = [Li^+]/[EO]$)
$\langle r_d^2(t) \rangle$	mean squared displacement
R	gas constant (8.314 J/molK)
T	absolute temperature (K)
T_h	thermodynamic factor
t_+^0	true cation transference number for non-ideal concentrated solutions
v_i	velocity of species i (cm/s)
x	cell coordinate defined such that $x = 0$ is at the anode and $x = L$ the cathode (μm)

Greek

γ_{+-}	mean molar activity coefficient of the salt
ϵ	dielectric constant
ε_0	permittivity of vacuum (8.854×10^{-12} C/Vm)
Φ	potential (V)
κ	ionic conductivity (S/cm)
$\nabla\mu_i$	gradient of the electrochemical potential of species i
τ_e	entanglement relaxation time
τ_R	Rouse time
τ_d	diffusive relaxation time for polymer chain
τ_D	diffusive relaxation time for ions
ζ	monomeric friction coefficient

1. Introduction

As we celebrate the 100th anniversary of the Macromolecular Hypothesis of Staudinger,[1] we recognize the numerous important ways in which polymers have affected our lives. Examples include the fuselages of modern airplanes, soft foams used in mattresses, rubber tires, and plastics that are used to make furniture, toys, and other items that are ubiquitous in society. Arguably, the most important unresolved issue of the day relates to the development of a clean and sustainable energy landscape. At this juncture, polymers play a minor role in this arena.

The question of how we will store and use energy in the future is an open one. In one scenario, we could generate energy using renewable but intermittent sources like the sun and the wind. If these are our only sources of energy, then we will need a device to store energy so that we may use it when the need arises. The lithium-ion battery is the only device available in the market that can serve this need. These batteries shot into prominence because they power handheld electronic devices. Many people use these devices to learn about the world and to communicate with one another. Lithium-ion batteries also power an increasing number of electric vehicles; many believe that emission-free transportation is an important step toward a new energy landscape. This review is related to the role polymers might play in next generation lithium-ion batteries.

State-of-the-art lithium-ion batteries comprise a transition metal oxide cathode (e.g. $LiCoO_2$), a graphite anode, and an electrolyte that is a mixture of organic solvents (e.g. dimethyl carbonate and ethylene carbonate) and a lithium salt (e.g. $LiPF_6$).[2-4] Polymers play a passive role in these batteries. Polyvinylidene difluoride (PVDF) is used as a glue that binds the cathode and anode particles into coherent electrodes. Porous polyolefin films are used as separators that prevent short-circuiting of the cell; the pores when filled with the electrolyte provide avenues for

ion transport. Although lithium-ion batteries have improved over the last few decades, there are important limitations. The limited cycle life of lithium-ion batteries is mainly due to the limited stability of the electrolyte. Parasitic side-reactions between the electrolyte and the electrodes, particularly side-reactions at the anode, result in the formation of unwanted products that diffuse to other parts of the cell and undergo further reactions. These side-reactions reduce capacity and ultimately shut off the electrochemical reactions that underlie the ability of the battery to deliver power.[5] New electrodes with higher potential differences and capacity have been suggested. However, their implementation in practical devices has been thwarted by the lack of a suitable electrolyte. The flammability and reactivity of the electrolyte can, under some conditions, lead to thermal runaway and explosive battery failure as the polyolefin separator melts and eventually burns.[6, 7] In some cases, it is speculated that metal filings initially located in the non-critical parts of the battery, become dislodged and enter the space between the electrodes, resulting in a short circuit that leads to an explosion.

Solid electrolytes may resolve some of the limitations of liquid-electrolyte-based lithium-ion batteries. They are likely to be less flammable than organic liquids. The products of deleterious side-reactions are less likely to diffuse and undergo further reactions due to the lack of mobility in the solid electrolytes and this may improve the cycle life. Once an all-solid-state battery is made and tested, it is unlikely that foreign macroscopic objects will find their way toward the ion transport pathways.

Many inorganic crystals and glasses exhibit lithium ion transport rates that are comparable to liquids.[8, 9] However, the brittle nature of these materials poses processing challenges. In addition, it is difficult to imagine how adhesive contact at the interface between the active electrode particles and these solid electrolytes can be maintained, given that the active particles contract and

expand as the batteries are cycled. Polymeric solid electrolytes can resolve issues related to mechanical and interfacial properties but lithium ion transport rates in these materials are much lower than that in the crystalline and glassy electrolytes.[10] The important unanswered question is this: what is the sequence of monomers that will give the most efficacious polymer electrolyte.[11] Before attempting to answer this question, it is important to agree on the definition of electrolyte efficacy.

More often than not, projections of the efficacy of electrolytes are based on a single transport property: ionic conductivity (κ). There are numerous reports on the effect of monomer structure on κ.[12-16] We have steadfastly avoided using the term conductivity in the preceding paragraphs because the efficacy of polymer electrolytes depends on three additional parameters that are seldom discussed. These parameters were first described by Onsager[17] and later formalized for battery applications by Newman.[18, 19] Polymer electrolytes covered in this review are similar to conventional electrolytes such as mixtures of organic solvents and a lithium salt. Such electrolytes are called "binary electrolytes" due to the presence of two mobile charged species, i.e., the cation and the anion.[19] However, many important characteristics of these electrolytes can only be reconciled when one recognizes the ternary nature of the system as it contains cations, anions, and "solvent" molecules. In this review, the species that solvates the salt is a neutral polymer. In the discussion below, we focus on the motion of the cation and anion through polymer matrices. We cannot, however, ignore the motion of the polymer segments and, perhaps, polymer chains.

2. Solvation and Brownian motion

In the absence of an electric potential, the translational diffusion of the three electrolyte components at the molecular level can be described as random walks due to Brownian motion. However, the motion of all of the species is coupled due to the constraints of charge neutrality and incompressibility. The space vacated by a diffusing cation must be filled by some combination of the anion and polymer segments due to incompressibility. If the random motion of cations produces a high positive charge at a certain location, electrostatic forces will attract the charge-compensating anions toward that location or the concentrated cations will diffuse away from that location. In other words, for all practical purposes, the electrolyte is electrically neutral. Violations of charge neutrality occur on distances smaller than the Debye length,[20] which for all known polymer electrolytes is a fraction of a nanometer.

In classical electrolytic solvents such as cyclic carbonates or water, the salt ions are dissociated due to the high dielectric constant of the medium. The extent of dissociation can be gauged by the magnitude of the Bjerrum length, *l*, which is the separation between unlike charges that results in an attractive energy equal to the thermal energy, *kT*, where *k* is the Boltzmann constant and *T* is absolute temperature,[21]

$$l = \frac{e_c^2}{4\pi\varepsilon_0 \epsilon kT}, \quad (1)$$

where e_c is the charge of an electron (1.602 x 10^{-19} C), ε_0 is the permittivity of vacuum [8.854 x 10^{-12} C/(Vm)], and ϵ is the dielectric constant of the medium. Substituting the dielectric constant for water, 80, one obtains l = 0.7 nm. At room temperature, water molecules are mobile, and this enables rapid motion of highly dissociated ions. Ion transport in simple electrolytes such as dilute aqueous KCl solutions are described by the Nernst-Planck formulation.[19] In this formulation, the ions are independent of each other in spite of the solution containing two oppositely charged

species. One can think of the ions diffusing freely in a background, akin to neutral molecules in an ideal gas. In Figure 1a, we show a picture of this simple situation. In this case, ion-ion interactions can be neglected.

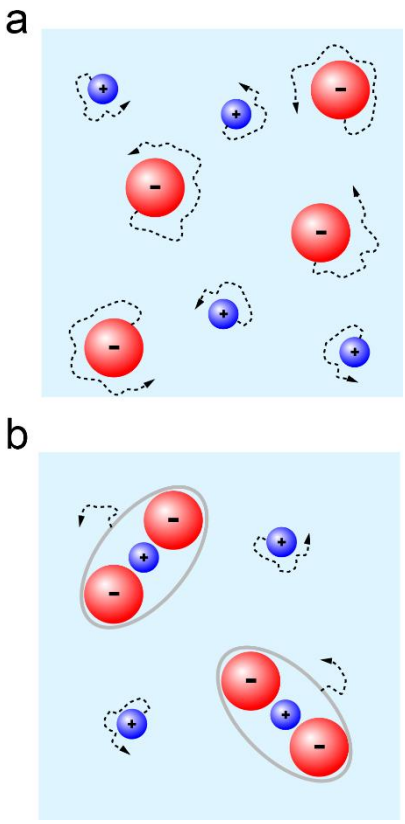

Figure 1. (a) Self-diffusion of fully dissociated ions. The Brownian motion of individual ions is uncoupled. (b) A more complex hypothetical situation where dissociation results in the formation of a cluster of two anions and one cation. The free cations are required due to electrical neutrality. In this case, the motion of the cations and the anions is intrinsically coupled.

Mobility of the solvating environment is essential for ion transport in binary electrolytes based on liquids and polymers. All known polymers with high dielectric constants consist of highly polar repeat units. The strong dipolar interactions hinder the mobility of the polymer segments.[22, 23] In a seminal paper [24], Fenton, Parker and Wright recognized that alkali metal salts could be dissolved in rubbery poly(ethylene oxide) (PEO), and the field of polymer

electrolytes was born. The dielectric constant of PEO is only 8.5, which gives l = 7.5 nm. Even in dilute mixtures, strong electrostatic forces will cause the average distance between pairs of positively and negatively charged ions to be considerably smaller than l. Mixtures of PEO and salt are thus thermodynamically non-ideal at all accessible salt concentrations. Even after 45 years

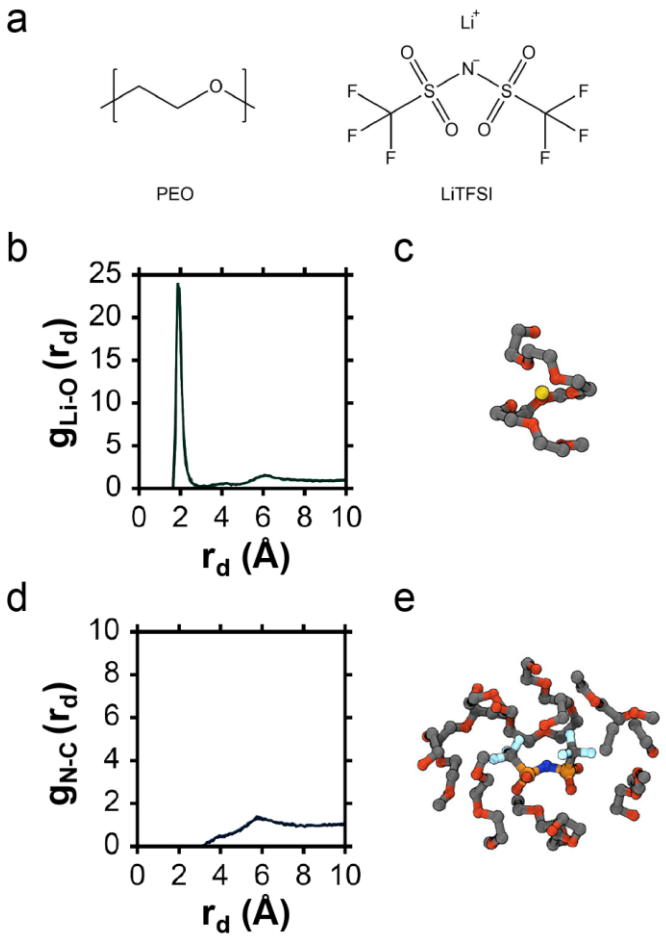

Figure 2. (a) Chemical structures of the solvent (PEO) and the salt (LiTFSI) (b) The cation-polymer radial distribution function, $g_{Li+-O}(r_d)$ and (c) a snap shot of the local environment near a Li^+ ion. (d) The anion-polymer radial distribution function, $g_{N-C}(r_d)$ and (e) the snap shot of the local environment near a $TFSI^-$ ion. [34], Copyright 2018. Adopted with permission from the American Chemical Society.

of study, many questions related to the distribution of salt ions in PEO matrices remain unresolved.[25-31] In Figure 1b, we show a picture where there are two "primary" charged species: free cations and clusters of two anions and a cation. Such clustering is not out of the question for complex systems such as PEO mixed with alkali metal salts.[32] It should be clear

that the Nernst-Plank formalism cannot be used to describe such systems. The dynamic nature of clusters that form and dissipate spontaneously, further complicates analysis of ion transport in non-ideal electrolytes.

In all electrolytes, the ions are surrounded by a solvation environment. In this work we focus on the best studied PEO-based electrolyte which contains lithium bis(trifluoromethanesulfonyl)imide (LiTFSI). The chemical structures of the electrolyte components are shown in Figure 2a. Molecular dynamics simulations reveal that in PEO/LiTFSI mixtures, a lithium ion is, on average, surrounded by six ether oxygens.[25, 33] The Li-O radial distribution function, $g_{\text{Li-O}}(r_d)$, exhibits a sharp peak at 2 Å, as shown in Figure 2b.[34] In addition to this dominant feature, a weak peak at 4 Å is observed before the function approaches unity with a broad shoulder at 6 Å. In contrast, the radial distribution function characterizing the anion surroundings is featureless; the N-C radial distribution function, $g_{\text{N-C}}(r_d)$, approaches unity with a broad shoulder at 6 Å as shown in Figure 2d. Figure 2c shows a typical conformation of PEO segments surrounding the Li^+ ion. All of the coordinating oxygens are derived from the same chain in this figure. Simulations show that sometimes two PEO chains provide the solvating environment; the number of chains solvating Li^+ is seldom greater than 2. A typical conformation of PEO segments surrounding the $TFSI^-$ ion, shown in Figure 2e, is similar to the conformation obtained in the absence of salt. One might hypothesize that the Brownian motion of the anion and cation would be significantly dissimilar due to differences in size and polymer segment distribution. The translation of Li^+ will involve rearrangement of the polymer segments in the newly occupied site as they will, on average, adopt conformations to surround the ion with its solvation environment until the ion diffuses away. The translation of a $TFSI^-$ ion does not, in principle, require such rearrangements.

3. Diffusion and migration under electric fields

In Figure 3 we show ideal ions (simple dissociation) in an electrolyte sandwiched between two lithium metal electrodes. In the absence of an applied electric field (Figure 3a), there is no ionic current flowing through the electrolyte and the ions exhibit Brownian diffusive motion as described in the preceding section. The random walk trajectories of the ions are shown by dashed lines in Figure 3a. In the absence of current, some cations may diffuse toward the positive electrode while other cations may diffuse toward the negative electrode, but the molar-average

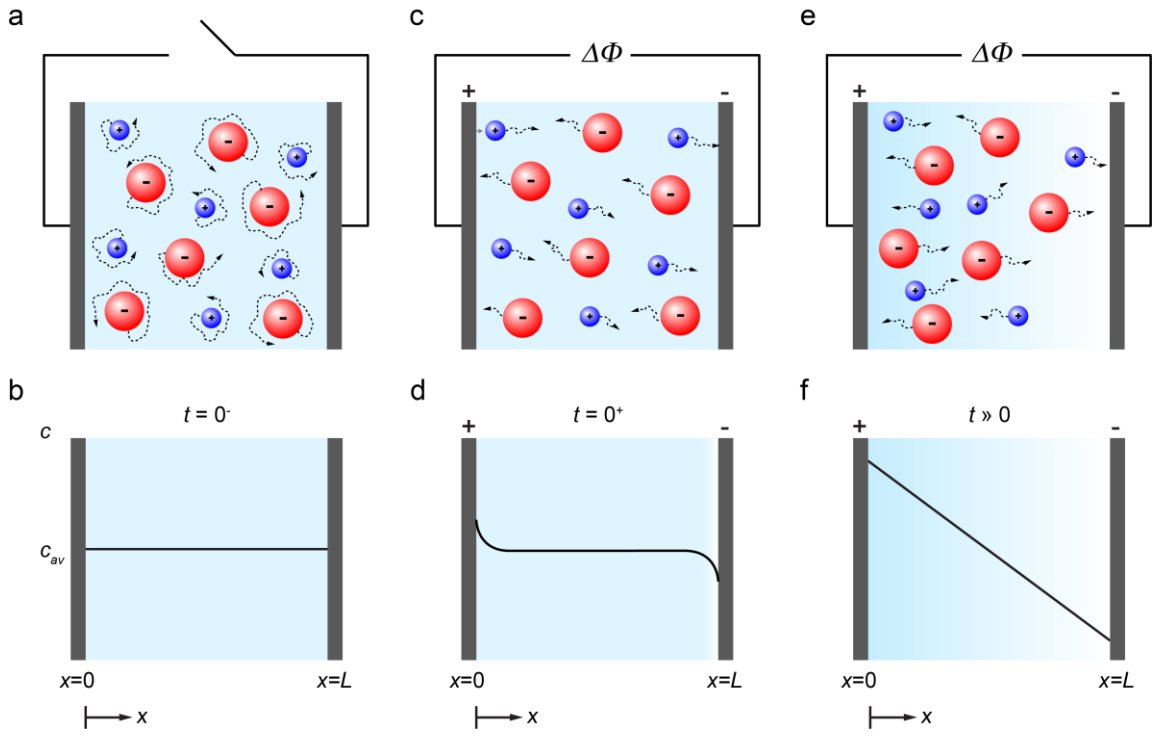

Figure 3. (a) Dissociated ions exhibit Brownian motion in the absence of an applied electric field. While individual ions move in particular directions, the average velocities of cations and anions are zero. (b) The salt concentration is thus uniform (c_{av}) from $x = 0$ to $x = L$. (c) As soon as the electric potential is applied ($t = 0^+$), the cations migrate toward the negative electrode ($x = L$) and the anions migrate toward the positive electrode ($x = 0$). (d) Concentration gradients start to form in the vicinity of the electrodes. (e) When steady state is reached, the cations migrate toward the negative electrode while the average velocity of the anion is zero. (f) A concentration gradient develops across the electrolyte. Polymer segments are not shown for clarity.

velocity of the cations, relative to the laboratory reference frame, in any particular direction is zero and the salt concentration in the cell is uniform as shown in Figure 3b.

The transport processes that occur when an ionic current flows through the polymer electrolyte under an applied electric potential differ substantially from self-diffusion. We apply a positive potential, $\Delta\Phi$, at $x = 0$, relative to the electrode at $x = L$. We refer to the positive electrode as the anode and the negative electrode as the cathode. While transport is still affected by the constraints of charge neutrality and incompressibility, as is the case in the absence of the applied field, the time-averaged velocities of the species are now space- and time-dependent. There are no concentration gradients at the first instant when a potential is imposed on the electrolyte ($t = 0^+$). In lithium batteries, lithium ions are released into the electrolyte at the anode/electrolyte interface ($x = 0$ in Figure 3) and withdrawn from the electrolyte at the cathode/electrolyte interface ($x = L$ in Figure 3). Charge neutrality requires the Li^+ fluxes at both electrodes to be equal at all times. Charge neutrality also requires the diffusion of anions toward the anode/electrolyte interface to "greet" the incoming cations at $t = 0^+$. Since anion fluxes into both electrodes are zero, overall mass balance implies depletion of the anions at $x = L$. Thus, at early times, the cations have a positive velocity while the anions have a negative velocity in the laboratory coordinate frame (Figure 3c). The negative velocity of the anions results in salt accumulation near $x = 0$ and depletion at $x = L$; the anion and cation concentrations must be equal at all x due to charged neutrality. At early times, the changes in salt concentration away from the average are localized near the electrodes (Figure 3d). As salt is depleted in the vicinity of $x = L$, polymer segments must take its place due to incompressibility. Similarly, as salt accumulates in the vicinity of $x = 0$, polymer segments must diffuse away from that region. All three components thus participate in ion transport during the early stages. With time, the spatial extent of the salt concentration gradient

increases until it takes over the entire cell. In the simplest case, a linear concentration profile is obtained at steady-state (Figure 3f). At steady-state, the net velocities of the anion and the polymer must be zero (boundary condition), while that of the cation is dictated by the imposed current. Note that the random-walk character of the displacement of individual ions is maintained under an applied field. However, when the average velocity of a large number of ions is determined at steady state, that of the cation is finite and positive while that of the anion is zero (Figure 3e). In other words, anion translation at steady state is similar to that obtained before the field is turned on. The term 'migration' is used to describe the effect of the electric field on the transport of ionic species, while the term 'diffusion' is used to describe transport due to non-uniform salt concentration. Both terms affect battery performance.

In Newman's concentrated solution theory, the species velocity obtained due to the presence of an electric field or a salt concentration gradient is governed by the following equations:[35]

$$\frac{\nabla\mu_+}{RT} = \frac{c_0}{c_T\mathfrak{D}_{0+}}(v_0 - v_+) + \frac{c}{c_T\mathfrak{D}_{+-}}(v_- - v_+), \quad (2)$$

$$\frac{\nabla\mu_-}{RT} = \frac{c_0}{c_T\mathfrak{D}_{0-}}(v_0 - v_-) + \frac{c}{c_T\mathfrak{D}_{+-}}(v_+ - v_-), \quad (3)$$

where $\nabla\mu_i$ is the gradient of the electrochemical potential of species *i*, *R* is the universal gas constant, *T* is the temperature, $\mathfrak{D}_{ij}$ is the Stefan-Maxwell diffusion coefficient describing interactions between species *i* and *j*, v_i and v_j are the net velocities of species *i* and *j*. The subscripts +, -, and 0 indicate cation, anion, and solvent. In addition, Eq. (2) and (3) contain three measures of salt concentration: molar salt concentration, *c*, the total concentration of the electrolyte defined as the sum of the moles of ethylene oxide monomers, lithium and TFSI ions per L of mixture, c_T, and the moles of ethylene oxide monomers per L of mixture, c_0. While Eq. (2) and

(3) apply to any reference frame, it is convenient to use the stationary reference frame of the battery. In the dilute limit, $c \to 0$, the first term on the right sides of Eq. (2) and (3) dominate. It is interesting to note that the application of an electric field may induce motion of a neutral species, i.e., v_0 may not be zero. This arises naturally due to coordination between the polymer and the ions: if the lithium ion in Figure 3c is driven to the right by an electric field, it is possible that some of the polymer segments will be dragged in that direction due to coordination described in Figure 2c.

4. Ion transport

Most batteries, especially those used in clean energy applications, are discharged slowly, over a time scale of one or more days. However, the reverse process, i.e., charging, is desired to be as quick as possible. The drive for discovering electrolytes is thus mainly to reduce charging time, and aimed at improving battery performance when it is used to power an electronic device or an electric vehicle. As the current fed into the battery during charging increases, the salt concentration gradients increase in magnitude. At a particular current, the salt concentration at the cathode drops to zero (for simplicity, we assume the cathode is planar as in Figure 3 and the cathode-electrolyte interface is located at $x = L$). This is called the limiting current.[19] It is obvious that the electrolyte with the higher limiting current (for a fixed electrode separation, L) is more efficacious as it places a limit on how fast a battery can be charged. The limiting current is governed by three transport coefficients, the Stefan-Maxwell diffusion coefficients, $\mathfrak{D}_{0+}, \mathfrak{D}_{0-}, \mathfrak{D}_{+-}$, and one thermodynamic parameter.[19] These four parameters have only been measured in PEO/LiTFSI mixtures in the vicinity of 90 ℃ thus far.[36] We therefore focus on the characterization of this system.

The transport and thermodynamic parameters discussed above are strong functions of the salt concentration. Concentration can be expressed in terms of molality, m, or molar concentration, c, or the ratio of lithium ions to ether oxygens, r. We use r to quantify salt concentration in this discussion. The relationship between r and other measures of concentration, i.e., c, c_0 and c_T for PEO/LiTFSI is given in Figure S1 (supporting information).

A powerful aspect of the framework that we describe here is that predictions of the limiting current can be made regardless of the molecular picture.[17-19] The Stefan-Maxwell diffusion coefficients and the thermodynamic factor will reflect the nature of ion dissociation in the electrolyte. In particular, if clusters such as those shown in Figure 1b are formed in the electrolyte, the ion velocities in Eq. (2) and (3) reflect the molar-average velocities of the free cation and the triplet.

The Stefan-Maxwell diffusion coefficients characterize transport on macroscopic (cell level) length scales. On the other hand, we are interested in the question, what monomers should be used in our polymerization reactions, a question that is related to the structure of the polymer on the Å scale. The discussion below covers all relevant length scales.

4.1. Salt chemical potential

The salt chemical potential of an electrolyte with univalent ions is given by [19]

$$\frac{\mu_{salt}}{RT} = 2\ln(m\gamma_{+-}) + \text{constant}, \quad (4)$$

where γ_{+-} is the mean molal salt activity coefficient. The constant depends on the secondary reference state used to define the free energy of the electrolyte and since we are only interested in

the gradient of chemical potential ($\nabla\mu_{salt}$), it is irrelevant. It is convenient to examine the concentration dependence of γ_{+-} instead of μ_{salt}, as the latter approaches -∞ in the dilute limit ($m \to 0$). It is convenient to define a thermodynamic factor, T_h, as

$$T_h = \left(1 + \frac{d \ln \gamma_{+-}}{d \ln m}\right), \quad (5)$$

because this term occurs naturally in the transport equations[19]. In Figure 4a, we plot T_h as a function of salt concentration of PEO/LiTFSI.[36] At low salt concentrations, T_h increases until a maximum is reached at r = 0.08. This is followed by a decrease to a minimum at r = 0.17. The reduction of salt activity as r = 0.17 is approached is interesting as this is the concentration at which all of the oxygens in PEO are associated with the available Li^+; recall each Li^+ is associated

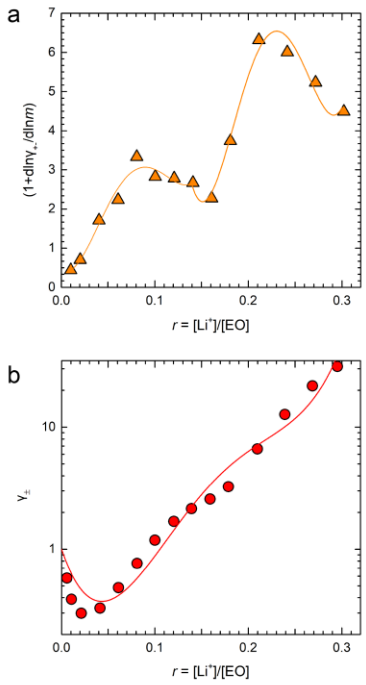

Figure 4. (a) The thermodynamic factor and (b) activity coefficient of PEO/LiTFSI as a function of salt concentration (r). The curves are 4th order polynomial fits, described in [36]. [36], Copyright 2018. Adopted with permission from the Electrochemical Society.

with 6 oxygens (Figure 2). At salt concentrations exceeding r = 0.17, T_h increases rapidly. In Figure 4b, we plot γ_{+-} as a function of salt concentration. This figure is obtained by integrating the data in Figure 4a with the boundary condition that γ_{+-} approaches 1 as r approaches 0. At low salt concentrations, γ_{+-}decreases with increasing salt concentration, reaching a minimum at r = 0.02, and then increases. The non-monotonic dependence of γ_{+-} on salt concentration in the dilute regime is similar to that seen in conventional electrolytes (aqueous HCl mixtures), and is attributed to charge screening which is generally described by the Debye-Hückel theory. [19]

4.2. Polymer and ion dynamical modes and experimental methods

The diffusion of long polymer chains in the neat state is described by the reptation model of de Gennes.[37] In this model, Brownian motion of the monomers in the direction perpendicular to the chain contour is severely restricted due to the presence of neighboring chains. This restriction is modeled by a tube of diameter a. The motion of the chains is described by a spectrum of relaxation times, as is always the case with chain-like molecules,

$$\tau_{D,p} = \left(\frac{\zeta}{\pi^2 kT}\right)\frac{b^4}{a^2}\frac{N^3}{p^2}, \quad (6)$$

where N is the number of monomers per chain, ζ is the friction coefficient between the monomers and the medium, k is the Boltzmann constant, b is the statistical segment length of the chains, and p is an integer between 1 and ∞. The statistical segment length of PEO in the neat state is 0.58 nm.[38] Reptation theory is valid when N exceeds a critical value called the entanglement threshold. The entanglement threshold for neat PEO is ~ 5 kg/mol.[39] Below this threshold, the entire spectrum of relaxation times is given by the Rouse model:

$$\tau_{R,p} = \left(\frac{\zeta}{\pi^2 kT}\right) b^2 \frac{N}{p^2}, \quad (7)$$

where p is an integer between 1 and N. We are primarily interested in the motion of ions in entangled PEO polymers where $M_n > 5$ kg/mol or $N > 110$ (N is the number of monomers based on a reference volume of 0.1 nm^3). In this range of chain length, the conductivity of PEO/LiTFSI mixtures is independent of N.[40, 41]

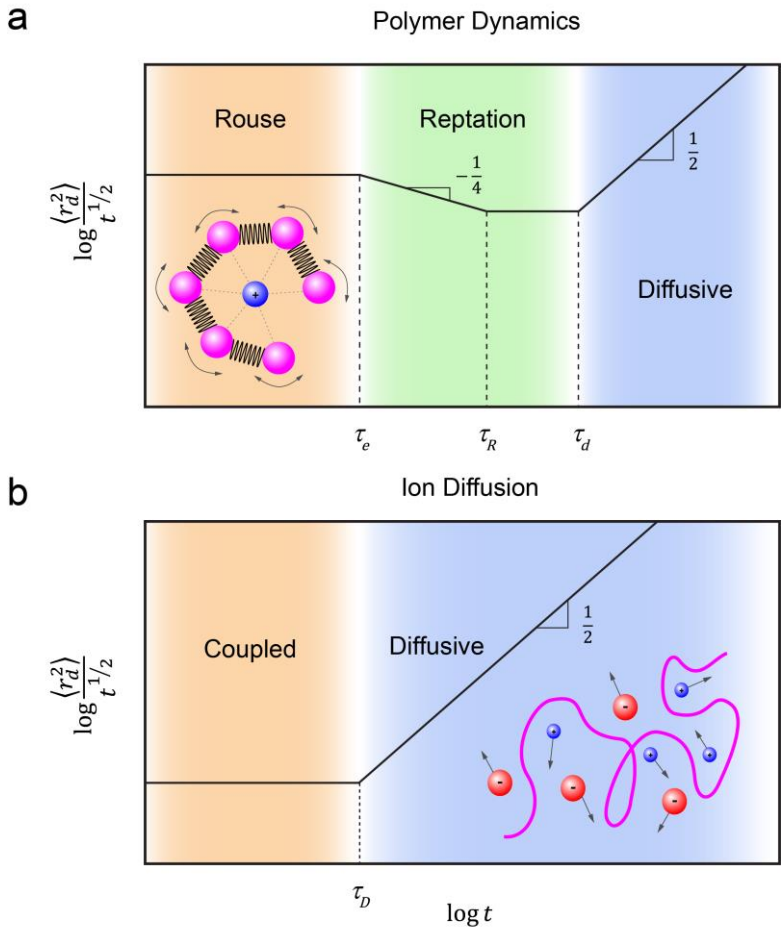

Figure 5. (a) Time-dependence of the mean squared displacement, $\langle r_d^2(t) \rangle$, of entangled polymers normalized by square root of time. At short time scales, $t < \tau_e$, segmental motion described by the Rouse model dominates. This motion is coupled to that of the cation as shown in the schematic. At intermediate times, $\tau_e < t < \tau_d$, segmental motion is restricted due to the presence of reptation tubes. At long times, $t > \tau_d$, center of mass diffusion of polymer is observed. (b) Time-dependence of the mean squared displacement of ions normalized by square root of time. At short time scales, $t < \tau_D$, sub-diffusive motion is observed. At longer times, $t > \tau_D$, ion motion is diffusive. Diffusive motion of ions on long time scales is dictated by Rouse motion of polymer segments on short time scales.

Insight into the nature of molecular motion can be obtained by examining the mean squared displacement of a monomer unit as a function of time t, $\langle r_d^2(t) \rangle$. The dependence of $\langle r_d^2(t) \rangle$ versus t for an entangled polymer melt (without salt) is shown in Figure 5a. At short times, relaxation is dominated by high p modes. In this limit, polymer segment motion is sub-diffusive and $\langle r_d^2(t) \rangle$ is proportional to $t^{1/2}$. This relationship is obtained by integrating all of the fast modes in Eq. (7). In this time window, it is convenient to define the Rouse parameter;

$$p_R = \frac{<r_d^2(t)>}{t^{1/2}}, \quad (8)$$

The Rouse parameter quantifies the short time sub-diffusive motion of polymer segments. The time scale over which Rouse dynamics is observed is so short that no effects of entanglement are evident.

On longer time scales, i.e. $t > \tau_e$, the motion of segments is restricted by the presence of the reptation tube, and $<r_d^2(t)>$ is proportional to $t^{1/4}$ (see Figure 5a). In this regime, $<r_d^2(t)>$ is a very weak function of time. On still longer time scales ($t > \tau_R$), the mean squared displacement of the monomer units is governed by the curvilinear diffusion of the chain and it is proportional to $t^{1/2}$. This mode of diffusion persists until the diffusive time, $t = \tau_d$. On time scales longer than τ_d, the chain finally escapes from the tube and the motion of segments is dominated by the diffusion of the center of mass of the chain. This is the diffusive regime and $<r_d^2>$ is proportional to t. The crossovers from one regime to the next are smooth; the boundaries between the different dynamical regimes in Figure 5a are shown by sharp dividing lines for clarity.

The spectrum of relaxation times based on the reptation model (Eq. (6)) describes chain motion on time scales greater than τ_R. The spectrum of relaxation times needed to describe chain motion on time scales smaller than τ_R are added in by hand, based on the expectation that Rouse type contour length fluctuations will emerge on time scales between τ_e and τ_R and that the Rouse modes will be obtained on still shorter time scales. Thus, the long-time plateau in Figure 5a is obtained by integrating fast reptation modes (Eq. (6)) while the short-time plateau in Figure 5a is obtained by integrating fast Rouse modes (Eq. (7)).[42, 43]

It is not clear how the regimes identified in Figure 5a are affected by the presence of salt. Current understanding suggests that these regimes will persist in polymer electrolytes but the time

scales (τ_e, τ_R, τ_d) will increase with the addition of salt due to association between the salt and the polymer chains. The addition of salt will certainly affect the monomeric friction coefficient, ζ, due to the coordination between polymer segments and the lithium ion.[44] Whether or not, the presence of salt induces other changes in the spectrum of relaxation times is unclear. The possibility of introducing new salt-induced relaxation modes is not entirely out of the question.

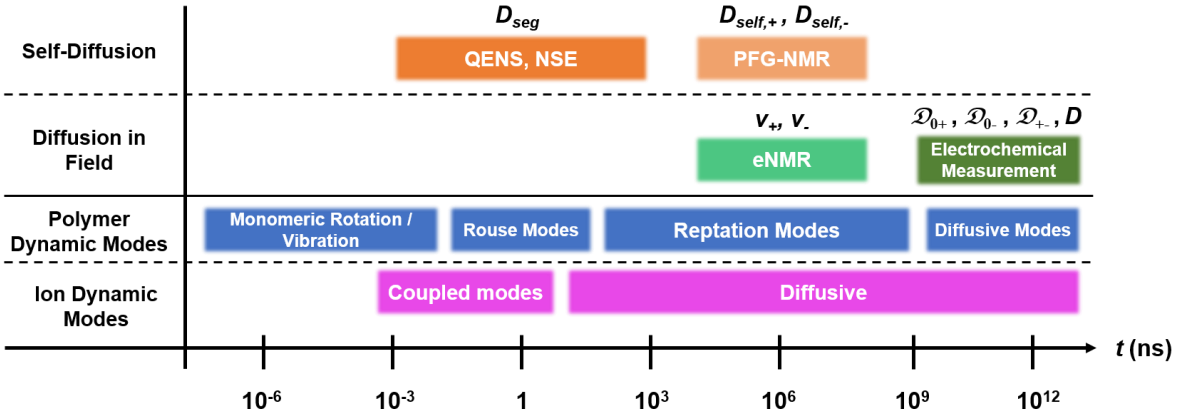

Figure 6. Time scales of the dynamical modes characterizing the mean squared displacement of polymers and ions shown in Figure 5. The experimental methods used to probe the different modes are also shown along with the transport parameters that are measured by experiments.

The diffusion of ions is, on paper, simpler than that of polymer chains. On short time scales ($t < \tau_D$), the motion is sub-diffusive and on long time scales, the motion is diffusive. Conventional wisdom suggests that ion diffusion is coupled to segmental motion of polymers on short time scales.[25, 45-47] The sub-diffusive mean squared displacement characteristics of the ions are thus assumed to be similar to that of the Rouse regime, as shown in Figure 5.[25] Simulation results[48] are qualitatively consistent with this assumption. However, experimental studies of sub-diffusive ion motion in polymer electrolytes have not yet been carried out.

Since we have two components that diffuse on disparate length and time scales, data from a variety of experimental methods are necessary to obtain a complete picture of ion transport in

polymer electrolytes. In Figure 6, we show typical time scales associated with the dynamical modes identified in Figure 5. Figure 6 also shows the relevant experimental methods for studying ion and polymer dynamics. In principle, one would like to know how the presence of ions affects all of the dynamical regimes of polymers. This is a multiscale problem outside the scope of this review. Instead, we acknowledge the practical fact that for electrolyte applications, we mainly care about ion dynamics. The crucial question is: what relaxation modes of polymer chains have a significant influence on ion dynamics. While we do not know the complete answer to this question, we do know that Rouse modes are important. These modes are studied by quasi-elastic neutron scattering (QENS). Dynamics on the time scale of tube diameter fluctuations are typically studied by neutron spin-echo (NSE) spectroscopy, but to our knowledge, there are no published reports of NSE data on polymer electrolytes. While it is clear that the presence of ions will affect standard rheological properties like storage and loss shear moduli, it is unclear if these properties affect ion motion significantly. However, rheological properties by themselves are important for practical applications as the electrolyte serves as a physical barrier between the two electrodes in a battery and thereby prevents shorting. Thus, the performance of a polymer-electrolyte-based battery is affected by the rheological properties of the electrolyte.

The self-diffusion of ions in the absence of electric fields is studied by pulsed-field gradient NMR (PFG-NMR).[49, 50] The emerging technique of electrophoretic NMR (eNMR) enables quantifying the migration velocities of ions and the polymer under applied electric fields.[51, 52] Finally, electrochemical measurements on different kinds of cells containing the electrolyte can be used to obtain Stefan-Maxwell diffusion coefficients. These coefficients in combination with the thermodynamic factor can be used to quantify the performance of the electrolytes in practical

batteries and predict parameters like the limiting current. They also enable prediction of migration velocities of the ions [35].

4.3.Polymer segmental dynamics

QENS is a powerful that exploits the large incoherent neutron scattering cross-section of hydrogen atoms and quantifies the motion of hydrogen-containing compounds on short time scales. Fortunately, most polymers contain hydrogen atoms and PEO is no exception. The length scales accessed by QENS lie between 0.5 and 5 nm, comparable to the statistical segment length *b*; the value of *b* based on a reference volume of 0.1 nm^3 is 0.5 ± 0.1 nm for a wide variety of polymers[53]. QENS is thus ideally suited for studying the Rouse regime (see Figures 5 and 6).

Figure 7a shows plots of experimentally measured $<r_d^2(t)>$ versus *t* of PEO/LiTFSI mixtures measured by QENS.[44, 54-56] The data shown were obtained at different salt concentrations. In most cases, $<r_d^2(t)>$ is proportional to $t^{1/2}$ as expected from theory; the dashed line in Figure 7a shows this scaling. The absolute value of $<r_d^2(t)>$ at a given time tends to decrease with increasing salt concentration. This is one manifestation of the slowing down of polymer segmental motion due to the presence of salt. At high salt concentrations, $r > 0.17$, $<r_d^2(t)>$ is a weaker function of time than the Rouse prediction. This is another observation related to the slowing down of segmental relaxation due to the presence of salt.

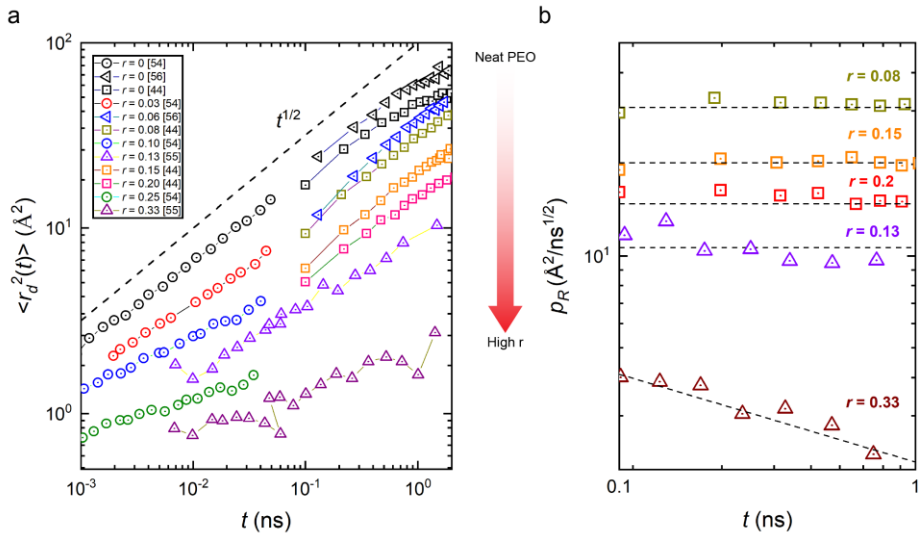

Figure 7. (a) Time-dependence of the mean squared displacement, $\langle r_d^2(t)\rangle$, of PEO/LiTFSI extracted from QENS. At low salt concentrations, $\langle r_d^2(t)\rangle$ scales linearly with $t^{1/2}$. However, at high salt concentrations, $r > 0.20$, different scaling is observed. (b) Time-dependence of the mean squared displacement, $\langle r_d^2(t)\rangle$, normalized by square root of time for selected electrolytes. At low salt concentrations, the horizontal fits through the data enable calculation of the Rouse parameter, p_R. At high salt concentrations, the data deviate from Rouse dynamics. Data taken from the literature. [44, 54 - 56].

In Figure 7b, we plot the Rouse parameter, p_R, determined from selected data sets in Figure 7a, as a function of t. The horizontal fits in Figure 7b are used to determine the average value of p_R which is used to calculate the segmental friction coefficient, ζ, [43, 57]

$$\zeta = \frac{12kTb^2}{p_R^2\pi} \quad , (9)$$

Generally speaking, the Rouse parameter decreases with increasing salt concentration, indicating that ζ increases, as expected. At the highest salt concentration $r = 0.33$, $\langle r_d^2(t)\rangle$ is no longer proportional to $t^{1/2}$. We posit that at this concentration, some of the Rouse relaxation times are outside the time window of the QENS experiments.

One can use the fluctuation-dissipation theorem[58] to define the polymer segmental diffusion coefficient

$$D_{seg} = \frac{kT}{\zeta} . \quad (10)$$

This may be interpreted as a fictitious diffusion coefficient associated with the polymer segments in these electrolytes if they could be freed from connectivity constraints and could diffuse freely. The reason for defining this diffusion coefficient will be made clear shortly.

4.4. Ion diffusion

The self-diffusion coefficients of ions, $D_{self,i}$, is given by,

$$D_{self,i} = \frac{<r_d^2(t)>}{6t} \qquad (i \text{ = + or -}), \quad (11)$$

These diffusion coefficients characterize ion motion in the absence of electric fields. A convenient experimental technique for measuring $D_{self,i}$ is PFG-NMR. In Figure 8a we plot the self-diffusion of Li^+ and $TFSI^-$ as a function of salt concentration. It should come as no surprise that $D_{self,+}$ is smaller than $D_{self,-}$, in spite of the fact that the anion is bulky. This is due to the coordination between PEO segments and the cation (Figure 2c) and the lack of coordination between PEO segments and the anion (Figure 2e).[59, 60] In addition, we also show D_{seg} as a function of salt concentration. Converting ζ obtained from sub-diffusive segmental motion into a diffusion coefficient (Eq. (10)) enables comparison of segmental polymer motion and ion diffusion on the same scale.

Stefan-Maxwell diffusion coefficients, $\mathfrak{D}_{ij}$, can be obtained by measuring the conductivity by ac impedance, the mutual salt diffusion coefficient by the restricted diffusion method, the steady current measured in a dc experiment, and data from concentration cells.[19, 61, 62] These experiments are conducted in cells with inter-electrode distances on the order of 100 μm. Details of the approach used in this review are given in ref. [36]. In Figure 8a we plot D_{seg}, $D_{self,+}$, $D_{self,-}$ and $\mathfrak{D}_{0+}$ as a function of salt concentration.[63] It is important to recognize the difference between these diffusion coefficients: D_{seg} reflects the motion of polymer segments on the 10^{-9} s time scale,

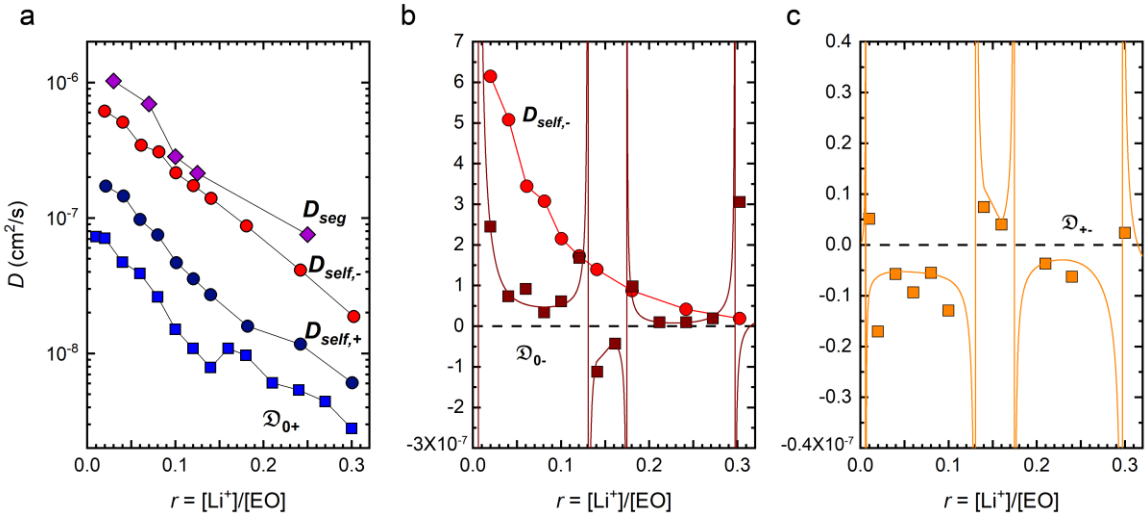

Figure 8. The dependence of diffusion coefficients on salt concentration, *r*, in PEO/LiTFSI. Rouse motion of polymer segments is quantified by D_{seg}, measured by QENS, the self-diffusion of cations and anions is quantified by $D_{self,+}$ and $D_{self,-}$, measured by PFG-NMR, and the build-up of concentration gradients in electrolytes under an applied potential is quantified by Stefan-Maxwell diffusion coefficients, $\mathfrak{D}_{0+}$, $\mathfrak{D}_{0-}$, and $\mathfrak{D}_{+-}$, measured by electrochemical characterization. Data taken from [36, 54, 63].

$D_{self,+}$ reflects the diffusion of Li^+ on the 10^{-3} s time scale, while $\mathfrak{D}_{0+}$ quantifies macroscopic motion of the cation in a cell with a characteristic time scale of 10^3 s. In spite of this, the four diffusion coefficients differ by only a factor of 10. More importantly, the salt concentration

dependencies of all four diffusion coefficients are more-or-less parallel. Since the lithium ions are strongly coordinated to the PEO segments (Figure 2c), one expects D_{seg} and $D_{self,+}$ to exhibit parallel trends. The fact that self-diffusion of the anions, $D_{self,-}$, is also parallel to D_{seg} is somewhat mysterious due to the lack of coordination between the polymer segments and the anions (Figure 2e). The formation and relaxation of concentration gradients in electrochemical cells depends on many parameters,[19] but surprisingly, the dependence of $\mathfrak{D}_{0+}$ on salt concentration is also parallel to that of D_{seg}. One may view all of the Stefan-Maxwell diffusion coefficients $\mathfrak{D}_{ij}$ as measures of friction between the species *i* and *j*. The agreement seen in Figure 8a suggests that friction between the cation and anion are unimportant; all aspects of ion transport covered in Figure 8a can essentially be explained by only considering the friction between the cation and the polymer segments. It is important to note, however, that the response of cations to concentration and potential gradients is affected by $\mathfrak{D}_{+-}$ (see Eq. (2)), a parameter that we have not yet discussed.

In Figure 8b, we focus on anion diffusion by comparing the dependencies of $D_{self,-}$ and $\mathfrak{D}_{0-}$ on salt concentration. Here we see dramatic differences. While $D_{self,-}$ decreases exponentially with added salt, $\mathfrak{D}_{0-}$ is non-monotonic function of salt concentration. It is positive at low concentrations, negative at intermediate concentrations, and positive at high concentrations. The division between these regimes are marked by singularities (poles). The regime where $\mathfrak{D}_{0-}$ is negative is particularly interesting as it indicates that the frictional interactions between the anion and polymer segments are non-trivial. These negative values force the use of a linear ordinate in Figure 8b.

When one of the Stefan-Maxwell diffusion coefficients is negative, it implies that contributions from the other relevant diffusion coefficient cannot be negligible. It is therefore instructive to examine the dependence of $\mathfrak{D}_{+-}$ on salt concentration which is shown in Figure 8c.

This plot is similar in character to the $\mathfrak{D}_{0-}$ plot, but the signs are opposite. This is required by the second law of thermodynamics as overall flux of a species must be in the direction of the gradient of the electrochemical potential (see Eq. (2) and (3)). The complex dependence of $\mathfrak{D}_{+-}$ on salt concentration indicates association between the cation and the anion. These effects may lead to the formation of clusters such as those shown in Figure 1b. If complex scenarios such as those shown in Figure 1b are present, then the Stefan-Maxwell diffusion coefficients represent averages over all of the different species present in the electrolyte. For example, in Figure 1b, we show the cation in two different states: free cations and negatively charged triplets. If this were true, then $\mathfrak{D}_{0+}$ would represent an average over the free cations and the triplets. However, the molecular underpinnings of $\mathfrak{D}_{0-}$ and $\mathfrak{D}_{+-}$ in PEO/LiTFSI mixtures remain to be established. Specifically, there is no experimental evidence for the presence of negatively charged triplets in PEO/LiTFSI mixtures.

4.5. Ion migration

The electrochemical potential gradient of the ions (left sides of Eq. (2) and (3)) can be caused by an applied electric field which leads to species migration, or a concentration gradient which leads to diffusion, or both. In this section, we focus on species velocities obtained under electric fields. We restrict ourselves to early times after applying the electric fields, i.e., when concentration gradients are confined to a small and insignificant region of the electrolyte, as is the case at time $t = 0^+$ in Figure 3e. Because the material properties are independent of position, the potential gradient is independent of position and we write:

$$\nabla\mu_+ = F\nabla\phi \ = -F\frac{\Delta\Phi}{L}, \quad (12)$$

and

$$\nabla\mu_{-} = F\frac{\Delta\Phi}{L}, \text{(13)}$$

In dilute electrolytes ($c \rightarrow 0$), the Eq. (2) and (3) reduce to

$$v_{+} - v_{0} = \frac{\mathfrak{D}_{0+}}{RT}\frac{F\Delta\Phi}{L}, \text{(14)}$$

which is positive and

$$v_{-} - v_{0} = -\frac{\mathfrak{D}_{0-}}{RT}\frac{F\Delta\Phi}{L}, \text{(15)}$$

which is negative (see coordinate frame defined in Figure 3); the diffusion coefficients must be positive in the limit of infinite dilution and the solvent velocity must be much smaller than the ion velocities.

At finite salt concentrations where the terms containing $\mathfrak{D}_{+-}$ are no longer negligible, expressions for the net species velocities at $t = 0^{+}$ are given by:[35]

$$v_{+} - v_{0} = \frac{c_T\mathfrak{D}_{0+}\mathfrak{D}_{+-}}{(c(\mathfrak{D}_{0-}+\mathfrak{D}_{0+})+c_0\mathfrak{D}_{+-})RT}\frac{F\Delta\Phi}{L}, \text{(16)}$$

$$v_{-} - v_{0} = \frac{-c_T\mathfrak{D}_{0-}\mathfrak{D}_{+-}}{(c(\mathfrak{D}_{0-}+\mathfrak{D}_{0+})+c_0\mathfrak{D}_{+-})RT}\frac{F\Delta\Phi}{L}, \text{(17)}$$

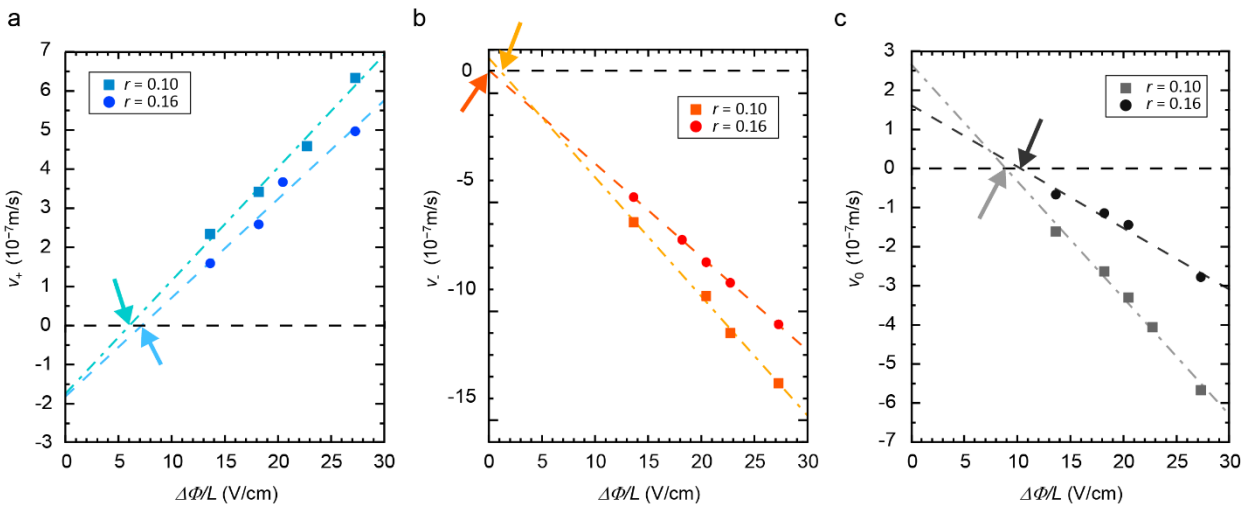

Figure 9. The velocities of (a, b) ions and (c) polymer as a function of potential gradient as measured by eNMR.[52] The velocity of the species is expected to be zero in the absence of the external field ($\Delta\Phi/L$=0). The dashed lines are least-square linear fits through the data. The arrows point to extrapolated intercepts of the data. Data taken from [52].

The molar averaged ion and polymer segment velocities in PEO/LiTFSI as a function of $\Delta\Phi/L$, measured recently by eNMR, for two salt concentrations are shown in Figure 9.[52] At both salt concentrations v_+ is positive while v_- is negative. An unexpected finding is that the measured v_+ values do not extrapolate to zero as the applied potential approaches zero. In contrast, the v_- data set do not exhibit this anomaly. The measured v_0 data are surprising in two respects: (1) the direction of v_0 is toward the positive electrode (same direction as v_-). Our understanding of coordination between the cation and PEO leads to the expectation of a positive v_0. (2) The measured v_0 values do not extrapolate to zero as the applied potential approaches zero. The observation that species velocities do not approach zero as the applied field approaches zero can only arise due to experimental artifacts. It is possible that in the experiments, ion motion is influenced by other factors such as natural convection due to resistive heating of the sample.

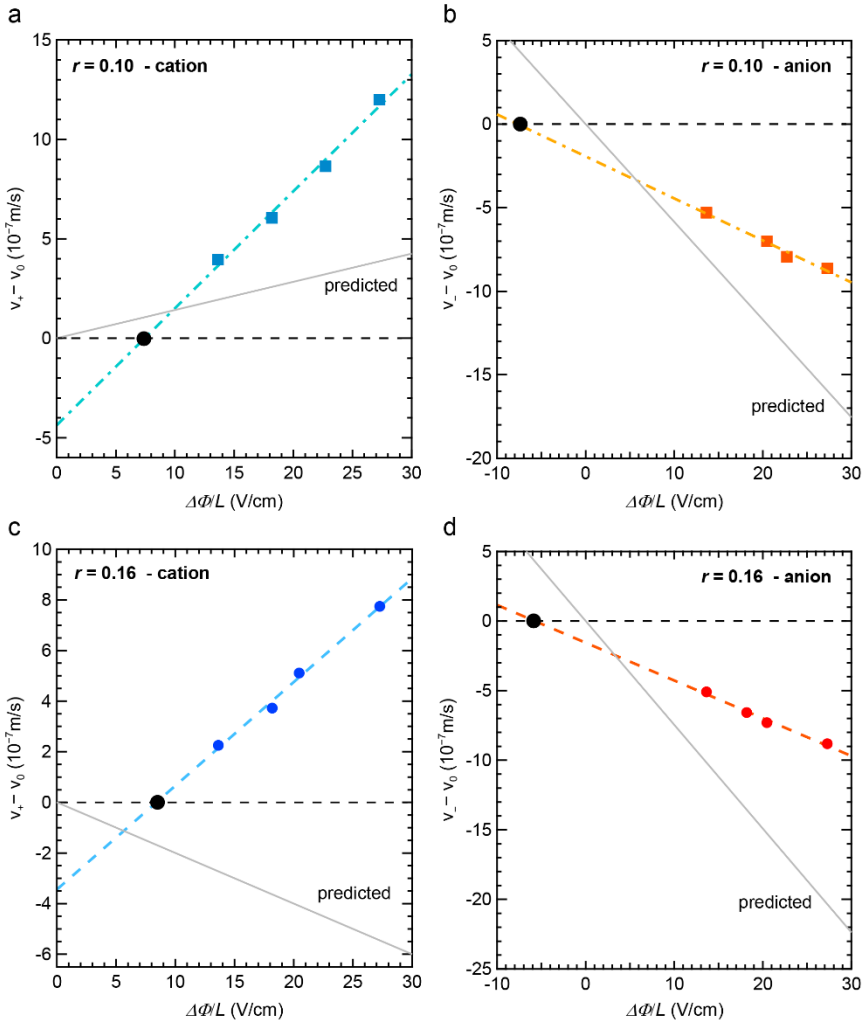

Figure 10. The velocities of ions relative to the polymeric solvent in PEO/LiTFSI as a function of potential gradient measured by eNMR.[52] The dashed lines are least-square linear fits through the data. The black circles show the extrapolated intercepts, i.e., the field at which the velocities of the ions relative to the solvent are zero. The solid lines are predictions based on Newman's concentrated solution theory and Stefan-Maxwell diffusion coefficients for PEO/LiTFSI (Figure 8). Data taken from [36, 52].

In Figure 10, we test the consistency of the data in Figure 9 with independently measured transport coefficients. The Stefan-Maxwell diffusion coefficients in Figure 8 are used to calculate the right sides of Eq. (16) and (17) as a function of the magnitude of the applied electric field, $\Delta\Phi/L$. The dotted lines in Figure 10 represent the results of these calculations. At r = 0.10, the calculated values of $(v_+ - v_0)$ are positive while those of $(v_- - v_0)$ are negative (Figures 10a and b). This is the expected situation pictured in Figure 3c when positive values of $\mathfrak{D}_{0+}$ and $\mathfrak{D}_{0-}$ dominate

ion transport. While the signs of the measured ion velocities relative to that of the solvent are identical to those predicted, the magnitudes differ by a factor of about two. A similar comparison between experiments and theory for $r = 0.16$ is presented in Figures 10c and d. The experimentally measured values of $(v_+ - v_0)$ and $(v_- - v_0)$ are positive and negative, respectively. In contrast, the theoretically predicted values of both $(v_+ - v_0)$ and $(v_- - v_0)$ are negative. In other words, both the cation and anion are predicted to migrate toward the positive electrode under an applied electric field (we assume the magnitude of v_0 is small compared to those of v_+ and v_-). In addition, the experimental data for $v_i - v_0$ (i = + or –) versus $\Delta\Phi/L$ do not pass through the origin. Further work is needed to resolve the discrepancy between theory and experiment in Figure 10.

We conclude this section by demonstrating a physical scenario that could result in the migration of both the cation and the anion toward the positive electrode. Consider applying an electric field on the electrolyte pictured in Figure 1b. In this relatively simple situation, at $t = 0^+$, the dissociated cation will migrate toward the negative electrode while the negatively charged cluster will migrate toward the positive electrode. While, the net velocity of the anion is positive in this scenario, the net velocity of the cation will depend on the mobility of the free cation relative to that of the cluster. If the dissociated cation is slower than the cluster, perhaps due to coordination between the cation and the polymer, then the net velocity of the cation will also be negative.[61, 64, 65]

4.6. Salt diffusion

One can define three overall salt diffusion coefficients:

$$\frac{1}{D_{self}} = \frac{1}{2}\left(\frac{1}{D_{self,+}} + \frac{1}{D_{self,-}}\right), \quad (18)$$

which reflects the self-diffusion of the ions,

$$\frac{1}{\mathfrak{D}} = \frac{1}{2}\left(\frac{1}{\mathfrak{D}_{0+}} + \frac{1}{\mathfrak{D}_{0-}}\right), \quad (19)$$

and the response of salt to a gradient in salt chemical potential, as well as a mutual diffusion coefficient, D, measured by restricted diffusion,

$$D = \mathfrak{D}\frac{c_T}{c_0}\left(1 + \frac{d\ln\gamma_{+-}}{d\ln m}\right). \quad (20)$$

Consider that two electrolyte chambers with salt concentrations $[c+\delta]$ and $[c-\delta]$ are brought in contact with each other (δ is small compared to c). Diffusion will drive the system so that the concentration in both chambers will be c in the limit of long times; D is the diffusion coefficient associated with this process.

The diffusion coefficients defined in Eq. (18) through (20) are always positive. In Figure 11, we plot D, $\mathfrak{D}$, and D_{self} of PEO/LiTFSI electrolytes as a function of salt concentration. While both $\mathfrak{D}$ and D_{self} decrease with increasing salt concentration, D, is more or less independent of salt concentration. It is clear that the addition of salt dramatically slows down ion motion. The reason for the qualitative difference between D and the other two diffusion coefficients is provided in Figure 4 where we see $1 + \frac{d\ln\gamma_{+-}}{d\ln m}$ increases with salt concentration. In other words, the activity coefficient is a more sensitive function of salt concentration as salt concentration increases. This increases the driving force for mutual diffusion at higher salt concentrations. In PEO/LiTFSI, the slowing down of ion motion due to the addition of salt is nearly exactly compensated for by the increase in $1 + \frac{d\ln\gamma_{+-}}{d\ln m}$.

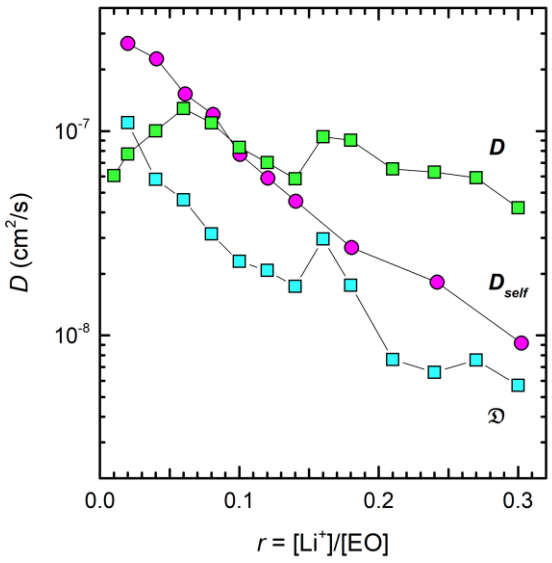

Figure 11. The dependence of three different salt diffusion coefficients on salt concentration, r. D_{self}, the self-diffusion coefficient measured by PFG-NMR, and $\mathfrak{D}$, the Stefan-Maxwell diffusion coefficient measured by electrochemical characterization decrease as the salt concentration increases while D, the diffusion coefficient measured by restricted diffusion is more-or-less independent of the salt concentration. Data taken from the literature [36, 63].

5. Connection to standard electrochemical characterization

The continuum properties of binary electrolytes are usually calculated using three transport properties: conductivity, κ, the salt diffusion coefficient, D; and the cationic transference number with respect to the solvent velocity, t_+^0.[18, 19, 61] Knowledge of these parameters is formally equivalent to knowledge of the Stefan-Maxwell diffusion coefficients, due to interrelationships between the two sets of parameters.

$$\frac{1}{\kappa} = \frac{RT}{c_T F^2}\left(\frac{1}{\mathfrak{D}_{+-}} + \frac{c_0(1-t_+^0)}{c\mathfrak{D}_{0-}}\right), \quad (21)$$

$$t_+^0 = \frac{\mathfrak{D}_{0+}}{\mathfrak{D}_{0+}+\mathfrak{D}_{0-}}, \quad (22)$$

In addition, t_+^0 can be formally expressed in terms of ion and polymer velocities measured at $t = 0^+$,

$$t_+^0 = \frac{v_+ - v_0}{v_+ - v_-}, \quad (23)$$

In this review, we use Stefan-Maxwell diffusion coefficients instead of κ, D, and t_+^0. The units of Stefan-Maxwell diffusion coefficients are the same as those obtained by QENS and PFG-NMR and this facilitates comparisons between ion transport data measured electrochemically with those measured by other approaches.

In the introduction, we suggest that the limiting current is the most important characteristic of an electrolyte. Experiments to determine the limiting current are conducted by imposing a fixed current on a cell similar to that depicted in Figure 3 and noting the steady voltage needed to sustain that current. Data obtained from such an experiment are shown in Figure 12.[66] Because the applied current in a cell is proportional to L, we use the product iL as the abscissa in Figure 12 to account for variations in L from cell to cell. The vertical line in the figure indicates the maximum current that could be imposed on the cell; when the applied current exceeded this value, the applied voltage needed to sustain this current increased exponentially with time. The curve in Figure 12 represents predictions based on the Stefan-Maxwell diffusion coefficients and the thermodynamic factor of that mixture. (The parameters used in reference [66] are very similar to those presented in Figures 4 and 8.) As the applied current is increased in the calculations, the predicted salt concentration at the cathode decreases. At the applied current density denoted by 'x' (iL=0.038 mA/cm) in Figure 12, the predicted salt concentration at the cathode is zero. The agreement between the measured limiting current and theoretical predictions seen in Figure 12 is encouraging.

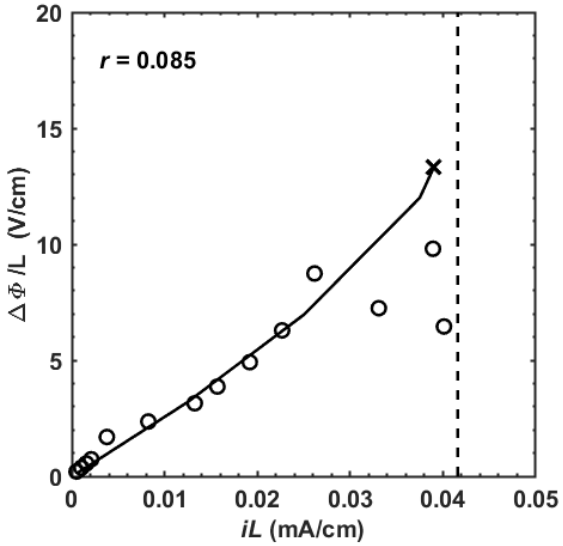

Figure 12. Steady-state potential normalized by the electrolyte thickness, $\Delta\Phi/L$, as a function of normalized current density, iL. When a normalized current density greater than 0.042 mA/cm is applied, the potential increases exponentially with time. The dashed line represents the experimentally determined limiting current for PEO/LiTFSI at r = 0.085. The solid line represents predictions based on Stefan-Maxwell diffusion coefficients. The 'x' indicates the theoretically predicted normalized limiting current. [66], Copyright 2019. Reproduced with permission from The Electrochemical Society.

6. Concluding remarks

Following the seminal work of Fenton *et al*.[24], numerous polymers were synthesized by the polymer community in the hope of obtaining "better" electrolytes than PEO/LiTFSI. Ideally, one would like a definitive answer to the question: what sequence of monomers would lead to a polymer that, when mixed with a lithium salt, selectively transports lithium ions at the highest rate? The purpose of this review is to outline the parameters that must be measured to answer this question. We accomplish this by summarizing what is known in the classic PEO/LiTFSI system. The framework described in this review is applicable to a binary mixture of any polymer and any salt.

We begin by noting that the sequence of monomers in the polymer will affect the solvation structure that surrounds the ions. This is reflected in the salt activity coefficient, γ_{+-}. Ion motion

is coupled to polymer segmental motion (D_{seg}) and independent of chain length. This is an important simplification and somewhat alien to polymer scientists, who tend to focus on properties that are controlled by chain length. The motion of segments is slowed down by the presence of the ions, and this slows down the self-diffusion of the ions ($D_{self,+}$ and $D_{self,-}$). Ion transport in electrochemical devices is ultimately characterized by three Stefan-Maxwell diffusion coefficients ($\mathfrak{D}_{0+}$, $\mathfrak{D}_{0-}$, and $\mathfrak{D}_{+-}$). The similar magnitude of D_{seg} $D_{self,+}$, $D_{self,-}$, and $\mathfrak{D}_{0+}$ over a wide range of salt concentration suggests that many important aspects of polymer electrolytes can be understood in terms of interactions between the lithium ions and the polymer (Figure 8a). Surprising discrepancies are evident in both magnitude and sign when $D_{self,-}$ is compared with $\mathfrak{D}_{0-}$ (Figure 8b). This discrepancy indicates complex interactions between the ions themselves and the ions and the polymer, and may be anticipated due to the large value of the Bjerrum length. Measurements of $\mathfrak{D}_{+-}$ confirm that this is true (Figure 8c). In hindsight, the agreement in Figure 8a is rather 'mysterious'. The relationship between ion migration and the applied electric field is even more mysterious. The difference in sign between the measured and calculated ($v_+ - v_0$) values (Figure 10) must be resolved.

We suggest that the limiting current (the product iL is independent of electrolyte thickness) in a standard cell is an excellent metric for quantifying the efficacy of different electrolytes. The widely used lithium-polymer-lithium symmetric cell seems to be an appropriate standard platform for measuring limiting current. However, designing new polymers with higher limiting currents is not trivial. Theoretical predictions of the limiting current require knowledge of the thermodynamic factor and all three Stefan-Maxwell diffusion coefficients. Rational design of polymer electrolytes will only be possible when the underpinnings of the relationships between

monomer structure and segmental motion, and those between segmental motion and Stefan-Maxwell diffusion coefficients are known.

Acknowledgement

This work was entirely supported by the Joint Center for Energy Storage Research (JCESR), an Energy Innovation Hub funded by the U.S. Department of Energy, Office of Science, Basic Energy Sciences.

References

[1] Staudinger H. Über Polymerisation. Ber Dtsch Chem Ges A, B Ser 1920;53:1073-85.

[2] Kim T, Song W, Son DY, Ono LK, Qi Y. Lithium-ion batteries: outlook on present, future, and hybridized technologies. J Mater Chem A 2019;7:2942-64.

[3] Goodenough JB, Park KS. The Li-ion rechargeable battery: a perspective. J Am Chem Soc 2013;135:1167-76.

[4] Li M, Lu J, Chen Z, Amine K. 30 Years of Lithium-Ion Batteries. Adv Mater 2018;30:1800561/1-24.

[5] Peled E, Menkin S. SEI: past, present and future. J Electrochem Soc 2017;164:A1703-A19.

[6] Xu W, Wang J, Ding F, Chen X, Nasybulin E, Zhang Y, Zhang JG. Lithium metal anodes for rechargeable batteries. Energy Environ Sci 2014;7:513-37.

[7] Fan X, Chen L, Borodin O, Ji X, Chen J, Hou S, Deng T, Zheng J, Yang C, Liou SC. Non-flammable electrolyte enables Li-metal batteries with aggressive cathode chemistries. Nat Nanotechnol 2018;13:715-22.

[8] Famprikis T, Canepa P, Dawson JA, Islam MS, Masquelier C. Fundamentals of inorganic solid-state electrolytes for batteries. Nat Mater 2019;18:1278-91.

[9] Bachman JC, Muy S, Grimaud A, Chang HH, Pour N, Lux SF, Paschos O, Maglia F, Lupart S, Lamp P, Giordano L, ShaoHorn Y. Inorganic Solid-State Electrolytes for Lithium Batteries: Mechanisms and Properties Governing Ion Conduction. Chem Rev 2016;116:140-62.

[10] Tarascon JM, Armand M. Issues and challenges facing rechargeable lithium batteries. Nature 2001;414:359-67.

[11] Ketkar PM, Shen KH, Hall LM, Epps TH. Charging toward improved lithium-ion polymer electrolytes: exploiting synergistic experimental and computational approaches to facilitate materials design. Mol Syst Des Eng 2019;4:223-38.

[12] Mindemark J, Lacey MJ, Bowden T, Brandell D. Beyond PEO—Alternative host materials for Li+-conducting solid polymer electrolytes. Prog Polym Sci 2018;81:114-43.

[13] Berthier C, Gorecki W, Minier M, Armand M, Chabagno J, Rigaud P. Microscopic investigation of ionic conductivity in alkali metal salts-poly (ethylene oxide) adducts. Solid State Ionics 1983;11:91-5.

[14] Papke B, Ratner M, Shriver D. Vibrational spectroscopy and structure of polymer electrolytes, poly (ethylene oxide) complexes of alkali metal salts. J Phys Chem Solids 1981;42:493-500.

[15] Perrier M, Besner S, Paquette C, Vallée A, Lascaud S, Prud'Homme J. Mixed-alkali effect and short-range interactions in amorphous poly (ethylene oxide) electrolytes. Electrochim acta 1995;40:2123-9.

[16] Brandell D, Priimägi P, Kasemägi H, Aabloo A. Branched polyethylene/poly (ethylene oxide) as a host matrix for Li-ion battery electrolytes: A molecular dynamics study. Electrochim Acta 2011;57:228-36.

[17] Onsager L. Theories and problems of liquid diffusion. Annal New York Acad Sci 1945;46:241-65.

[18] Doyle M, Fuller TF, Newman J. Modeling of Galvanostatic Charge and Discharge of the Lithium/Polymer/Insertion Cell. J Electrochem Soc 1993;140:1526-33.

[19] Newman J, Thomas-Alyea KE. Electrochemical systems. New York: John Wiley & Sons, 2012. 648 pp.

[20] Smith AM, Lee AA, Perkin S. The Electrostatic Screening Length in Concentrated Electrolytes Increases with Concentration. J Phys Chem 2016;7:2157-63.

[21] Bjerrum N. Ionic association. I. Influence of ionic association on the activity of ions at moderate degrees of association Danske Vid Selskab, Math-fys medd 1926;7:1-48.

[22] Wheatle BK, Lynd NA, Ganesan V. Effect of Polymer Polarity on Ion Transport: A Competition between Ion Aggregation and Polymer Segmental Dynamics. ACS Macro Lett 2018;7:1149-54.

[23] Wheatle BK, Keith JR, Mogurampelly S, Lynd NA, Ganesan V. Influence of Dielectric Constant on Ionic Transport in Polyether-Based Electrolytes. ACS Macro Lett 2017;6:1362-7.

[24] Fenton DE, Parker JM, Wright PV. Complexes of alkali metal ions with poly(ethylene oxide). Polymer 1973;14:589-9.

[25] Borodin O, Smith GD. Mechanism of Ion Transport in Amorphous Poly(ethylene oxide)/LiTFSI from Molecular Dynamics Simulations. Macromolecules 2006;39:1620-9.

[26] Pesko DM, Webb MA, Jung Y, Zheng Q, Miller TF, Coates GW, Balsara NP. Universal Relationship between Conductivity and Solvation-Site Connectivity in Ether-Based Polymer Electrolytes. Macromolecules 2016;49:5244-55.

[27] Webb MA, Savoie BM, Wang ZG, Miller III TF. Chemically Specific Dynamic Bond Percolation Model for Ion Transport in Polymer Electrolytes. Macromolecules 2015;48:7346-58.

[28] Savoie BM, Webb MA, Miller TF. Enhancing Cation Diffusion and Suppressing Anion Diffusion via Lewis-Acidic Polymer Electrolytes. J Phys Chem 2017;8:641-6.

[29] Diddens D, Heuer A, Borodin O. Understanding the Lithium Transport within a Rouse-Based Model for a PEO/LiTFSI Polymer Electrolyte. Macromolecules 2010;43:2028-36.

[30] Brooks DJ, Merinov BV, Goddard WA, Kozinsky B, Mailoa J. Atomistic Description of Ionic Diffusion in PEO–LiTFSI: Effect of Temperature, Molecular Weight, and Ionic Concentration. Macromolecules 2018;51:8987-95.

[31] Maitra A, Heuer A. Cation Transport in Polymer Electrolytes: A Microscopic Approach. Phys Rev Lett 2007;98:227802/1-4.

[32] Molinari N, Mailoa JP, Kozinsky B. Effect of Salt Concentration on Ion Clustering and Transport in Polymer Solid Electrolytes: A Molecular Dynamics Study of PEO–LiTFSI. Chem Mater 2018;30:6298-306.

[33] Diddens D, Paillard E, Heuer A. Improving the lithium ion transport in polymer electrolytes by functionalized ionic-liquid additives: simulations and modeling. J Electrochem Soc 2017;164:E3225-E31.

[34] Zheng Q, Pesko DM, Savoie BM, Timachova K, Hasan AL, Smith MC, Miller TF, Coates GW, Balsara NP. Optimizing Ion Transport in Polyether-Based Electrolytes for Lithium Batteries. Macromolecules 2018;51:2847-58.

[35] Timachova K, Newman J, Balsara NP. Theoretical Interpretation of Ion Velocities in Concentrated Electrolytes Measured by Electrophoretic NMR. J Electrochem Soc 2019;166:A264-A7.

[36] Villaluenga I, Pesko DM, Timachova K, Feng Z, Newman J, Srinivasan V, Balsara NP. Negative Stefan-Maxwell Diffusion Coefficients and Complete Electrochemical Transport Characterization of Homopolymer and Block Copolymer Electrolytes. J Electrochem Soc 2018;165:A2766-A73.

[37] de Gennes PG. Reptation of a polymer chain in the presence of fixed obstacles. J Chem Phys 1971;55:572-9.

[38] Niedzwiedz K, Wischnewski A, Pyckhout-Hintzen W, Allgaier J, Richter D, Faraone A. Chain Dynamics and Viscoelastic Properties of Poly(ethylene oxide). Macromolecules 2008;41:4866-72.

[39] Mark JE, editor. Physical properties of polymers handbook. New York: Springer Verlag, 2007. 1076 pp.

[40] Teran AA, Tang MH, Mullin SA, Balsara NP. Effect of molecular weight on conductivity of polymer electrolytes. Solid State Ionics 2011;203:18-21.

[41] Shi J, Vincent CA. The effect of molecular weight on cation mobility in polymer electrolytes. Solid State Ionics 1993;60:11-7.

[42] Watanabe H. Viscoelasticity and dynamics of entangled polymers. Prog Polym Sci 1999;24:1253-403.

[43] Doi M. Introduction to polymer physics. Oxford: Oxford university press, 1996. 148 pp.

[44] Mongcopa KIS, Tyagi M, Mailoa JP, Samsonidze G, Kozinsky B, Mullin SA, Gribble DA, Watanabe H, Balsara NP. Relationship between Segmental Dynamics Measured by Quasi-Elastic Neutron Scattering and Conductivity in Polymer Electrolytes. ACS Macro Lett 2018;7:504-8.

[45] Bresser D, Lyonnard S, Iojoiu C, Picard L, Passerini S. Decoupling segmental relaxation and ionic conductivity for lithium-ion polymer electrolytes. Mol Syst Des Eng 2019;4:779-92.

[46] Nitzan A, Ratner MA. Conduction in polymers: dynamic disorder transport. J Phys Chem 1994;98:1765-75.

[47] Druger SD, Nitzan A, Ratner MA. Dynamic bond percolation theory: A microscopic model for diffusion in dynamically disordered systems. I. Definition and one-dimensional case. J Chem Phys 1983;79:3133-42.

[48] Webb MA, Jung Y, Pesko DM, Savoie BM, Yamamoto U, Coates GW, Balsara NP, Wang ZG, Miller TF. Systematic Computational and Experimental Investigation of Lithium-Ion Transport Mechanisms in Polyester-Based Polymer Electrolytes. ACS Cent Sci 2015;1:198-205.

[49] Gorecki W, Roux C, Clémancey M, Armand M, Belorizky E. NMR and Conductivity Study of Polymer Electrolytes in the Imide Family: P(EO)/Li[N(SO2CnF2n+1)(SO2CmF2m+1)]. ChemPhysChem 2002;3:620-5.

[50] Donoso JP, Bonagamba TJ, Panepucci HC, Oliveira LN, Gorecki W, Berthier C, Armand M. Nuclear magnetic relaxation study of poly(ethylene oxide)–lithium salt based electrolytes. J Chem Phys 1993;98:10026-36.

[51] Zhang Z, Madsen LA. Observation of separate cation and anion electrophoretic mobilities in pure ionic liquids. J Chem Phys 2014;140:084204/1-10.

[52] Rosenwinkel MP, Schönhoff M. Lithium Transference Numbers in PEO/LiTFSA Electrolytes Determined by Electrophoretic NMR. J Electrochem Soc 2019;166:A1977-A83.

[53] Eitouni HB, Balsara NP. Thermodynamics of polymer blends. In: Mark JE, editor. Physical Properties of Polymers Handbook. New York: Springer, 2007. p. 339-56.

[54] Fullerton-Shirey SK, Maranas JK. Effect of LiClO4 on the Structure and Mobility of PEO-Based Solid Polymer Electrolytes. Macromolecules 2009;42:2142-56.

[55] Mao G, Saboungi ML, Price DL, Armand M, Mezei F, Pouget S. α-Relaxation in PEO−LiTFSI Polymer Electrolytes. Macromolecules 2002;35:415-9.

[56] Chen XC, Sacci RL, Osti NC, Tyagi M, Wang Y, Palmer MJ, Dudney NJ. Study of segmental dynamics and ion transport in polymer–ceramic composite electrolytes by quasi-elastic neutron scattering. Mol Syst Des Eng 2019;4:379-85.

[57] Rouse PE. A Theory of the Linear Viscoelastic Properties of Dilute Solutions of Coiling Polymers. J Chem Phys 1953;21:1272-80.

[58] Chandler D. Introduction to modern statistical mechanics. Oxford: Oxford University Press, 1987. p. 288 pp.

[59] Hayamizu K, Akiba E, Bando T, Aihara Y, Price WS. NMR Studies on Poly(ethylene oxide)-based Polymer Electrolytes with Different Cross-Linking Doped with LiN(SO2CF3)2. Restricted Diffusion of the Polymer and Lithium Ion and Time-Dependent Diffusion of the Anion. Macromolecules 2003;36:2785-92.

[60] Hayamizu K, Akiba E, Bando T, Aihara Y. 1 H, 7 Li, and 19 F nuclear magnetic resonance and ionic conductivity studies for liquid electrolytes composed of glymes and

polyetheneglycol dimethyl ethers of CH 3 O (CH 2 CH 2 O) n CH 3 (n= 3–50) doped with LiN (SO 2 CF 3) 2. J Chem Phys 2002;117:5929-39.

[61] Ma Y, Doyle M, Fuller TF, Doeff MM, De Jonghe LC, Newman J. The measurement of a complete set of transport properties for a concentrated solid polymer electrolyte solution. J Electrochem Soc 1995;142:1859-68.

[62] Pesko DM, Timachova K, Bhattacharya R, Smith MC, Villaluenga I, Newman J, Balsara NP. Negative transference numbers in poly (ethylene oxide)-based electrolytes. J Electrochem Soc 2017;164:E3569-E75.

[63] Timachova K. Ion Diffusion and Electrochemically Driven Transport in Homogenous and Nanostructured Polymer Electrolytes. PhD Thesis: UC Berkeley, 2018. 136 pp.

[64] France-Lanord A, Grossman JC. Correlations from Ion Pairing and the Nernst-Einstein Equation. Phys Rev Lett 2019;122:136001/1-6.

[65] Kraaijeveld G, Wesselingh JA. Negative Maxwell-Stefan diffusion coefficients. Ind Eng Chem Res 1993;32:738-42.

[66] Gribble DA, Frenck L, Shah DB, Maslyn JA, Loo WS, Mongcopa KIS, Pesko DM, Balsara NP. Comparing Experimental Measurements of Limiting Current in Polymer Electrolytes with Theoretical Predictions. J Electrochem Soc 2019;166:A3228-A34.